Structure of a protective epitope reveals the importance of acetylation of *Neisseria meningitidis* serogroup A capsular polysaccharide

Pedro Henriques[a,b], Lucia Dello Iacono[b], Ana Gimeno[c], Alessia Biolchi[b], Maria Rosaria Romano[b], Ana Arda[c], Gonçalo J. L. Bernardes[a,d], Jesus Jimenez-Barbero[c,e,f], Francesco Berti[b], Rino Rappuoli[b,1], and Roberto Adamo[b,1]

[a]Instituto de Medicina Molecular João Lobo Antunes, Faculdade de Medicina, Universidade de Lisboa, 1649-028 Lisboa, Portugal; [b]Research and Development Centre, GlaxoSmithKline (GSK), 53100 Siena, Italy; [c]Chemical Glycobiology Lab CIC bioGUNE Technology Park, 48160 Derio, Spain; [d]Department of Chemistry, University of Cambridge, CB2 1EW Cambridge, United Kingdom; [e]Ikerbasque, Basque Foundation for Science, 48013 Bilbao, Bizkaia, Spain; and [f]Department of Organic Chemistry II, University of the Basque Country, Universidad del País Vasco/Euskal Herriko Unibertsitatea, 48940 Leioa, Bizkaia, Spain

Contributed by Rino Rappuoli, August 27, 2020 (sent for review June 11, 2020; reviewed by Geert-Jan Boons and Emil C. Gotschlich)

Meningococcal meningitis remains a substantial cause of mortality and morbidity worldwide. Until recently, countries in the African meningitis belt were susceptible to devastating outbreaks, largely attributed to serogroup A *Neisseria meningitidis* (MenA). Vaccination with glycoconjugates of MenA capsular polysaccharide led to an almost complete elimination of MenA clinical cases. To understand the molecular basis of vaccine-induced protection, we generated a panel of oligosaccharide fragments of different lengths and tested them with polyclonal and monoclonal antibodies by inhibition enzyme-linked immunosorbent assay, surface plasmon resonance, and competitive human serum bactericidal assay, which is a surrogate for protection. The epitope was shown to optimize between three and six repeating units and to be *O*-acetylated. The molecular interactions between a protective monoclonal antibody and a MenA capsular polysaccharide fragment were further elucidated at the atomic level by saturation transfer difference NMR spectroscopy and X-ray crystallography. The epitope consists of a trisaccharide anchored to the antibody via the *O*- and *N*-acetyl moieties through either H-bonding or CH–π interactions. In silico docking showed that 3-*O*-acetylation of the upstream residue is essential for antibody binding, while *O*-acetate could be equally accommodated at three and four positions of the other two residues. These results shed light on the mechanism of action of current MenA vaccines and provide a foundation for the rational design of improved therapies.

carbohydrates | structural glycobiology | *Neisseria meningitidis* | vaccines

Capsular and other surface polysaccharides (PS) are major virulence components on bacterial cell surfaces and play critical roles in immune system evasion, acting as the primary interface for the host cells, and thus are considered attractive vaccine targets (1, 2). Mapping glycan antigenic determinants, recognized by bactericidal antibodies mediating protection from microbial infections, is of paramount importance to reveal suitable antigenic structures for immune response elicitation (3). However, the glycotope determinants and their bioactive conformations responsible for immunologic events are poorly understood, owing to the intrinsic flexibility and heterogeneity of bacterial PS.

Recent advances in carbohydrate synthesis, providing access to well-defined glycans, together with high-throughput glycoarrays or microfluidic tools, such as surface plasmon resonance (SPR), have fast tracked the screening of glycan-based antigens against different pathogens, such as *Clostridium difficile* (4) and *Streptococcus pneumoniae* (5). Structural identification of epitope determinants and their conformations can be attained in solution by NMR spectroscopy augmented by molecular dynamics (6), as recently featured in the development of a vaccine candidate against *Burkholderia pseudomallei* (7, 8). Paratope-epitope molecular determinants of interactions can be further disentangled at atomic resolution by X-ray crystallography. However, crystallization of glycan-Fab complexes has proven to be far more challenging than crystallization of protein antigen-Fab complexes, putatively due to glycan's greater flexibility and lower affinity compared with proteins (9). Over the past decades, several examples of glycan structural epitopes resolved at atomic resolution by X-crystallography have been reported, including *Salmonella typhimurium* lipopolysaccharide (10), *Vibrio cholerae* O1 (11), *Shigella flexneri* serotype 2a O-antigen (12), *Mycobacterium tuberculosis* PS (13), and group B *Streptococcus* PS (14). Understanding the structural basis of antigen-antibody binding events offers the promise for a guided rational design of innovative synthetic vaccines (15, 16), and glycomimetics (17, 18).

Invasive meningococcal disease is a daunting public health concern, mainly because of its rapid clinical onset. Historically, MenA has been considered a primary causative agent of sporadic and epidemic outbreaks, especially in the so-called "meningitidis belt" (19). An incidence of 10 to 1,000 cases per 100,000 population was reported (20), with MenA responsible for 70% to 96% of the cases before 2010 (21). Collective efforts in the

Significance

The elucidation of structural epitopes is key to understanding the mechanisms of action of vaccines. Here a multidisciplinary approach was used to map the glycan epitope of *Neisseria meningitidis* serogroup A capsular polysaccharide, a component of marketed vaccines, with a monoclonal antibody capable of triggering human complement-mediated bactericidal killing. The epitope was found to be composed of a trisaccharide motif, in which acetylation moieties play a pivotal role in binding. This study will guide the design of improved vaccines and therapeutics.

Author contributions: P.H., J.J.-B., F.B., and R.A. designed research; P.H., L.D.I., A.B., A.A., and J.J.-B. performed research; P.H., L.D.I., A.G., A.B., M.R.R., A.A., G.J.L.B., J.J.-B., R.R., and R.A. analyzed data; and P.H., L.D.I., A.A., F.B., and R.A. wrote the paper.

Reviewers: G.-J.B., University of Georgia; and E.C.G., The Rockefeller University.

Competing interest statement: P.H. is a student at the Instituto de Medicina Molecular João Lobo Antunes, Faculdade de Medicina, Universidade de Lisboa and participated in a postgraduate studentship program at GlaxoSmithKline (GSK). L.D.I., A.B., M.R.R., F.B., R.R., and R.A. are employees of the GSK group of companies. F.B., R.R., and R.A. are shareholders of the GSK group of companies. R.A. and F.B. are listed as inventors on a patent filed by GSK. A.G., A.A., G.J.L.B., and J.J.-B. have nothing to disclose.

[1]To whom correspondence may be addressed. Email: rino.r.rappuoli@gsk.com or roberto.x.adamo@gsk.com.

This article contains supporting information online at https://www.pnas.org/lookup/suppl/doi:10.1073/pnas.2011385117/-/DCSupplemental.

First published November 6, 2020.

PATH project with the development of MenAfriVac (22), along with vaccination campaigns, resulted in a disease incidence reduction of >99% (23).

MenA capsular PS is composed of *N*-acetyl-D-mannosamine moieties, α (1→6)-linked through phosphodiester linkages and partly *O*-acetylated at C-3 or C-4 (24–26). Early studies proposed that glycan chain length and *O*-acetylation pattern as key parameters for optimal immunogenicity of MenA vaccines. A Phase I clinical trial of a MenA oligosaccharide (OS) with an average chain length of 6 to 10 repeating units (RUs) conjugated to the diphtheria toxoid CRM_{197} showed it to be both safe and immunogenic (27). In contrast to many surface PSs, including those from *Shigella* spp and other meningococcal serogroups (28), *O*-acetylation has been hypothesized to play a critical role in MenA PS immunogenicity (29). Antibodies from immunized subjects were shown to preferentially recognize *O*-acetylated moieties, while de-*O*-acetylated PS conjugate resulted in a marked reduction of immunogenicity and, crucially, of the ability to induce bactericidal antibodies in murine models (30). Recently, in silico models have shown that MenA PS is presented either as an extended conformation or as a compact hairpin bend, with the conformational preference modulated by *O*-acetylation (31). Importantly, *O*-acetyl groups are solvent-exposed, making them accessible for intermolecular interactions (32).

Starting from this evidence, we envisaged the study of the interactions between MenA PS and bactericidal antibodies as a powerful means to provide insight into key immunologic determinants of this PS. We applied a combination of complementary techniques to map the structural epitope of *O*-acetylated MenA PS. A panel of MenA OSs of different lengths was generated by depolymerization of MenA plain PS, and competitive enzyme-linked immunosorbent assay (ELISA) and SPR were used to assess inhibition and binding kinetics to a bactericidal mAb. Saturation transfer difference (STD)-NMR, X-ray crystallography, and molecular dynamics were exploited to unravel the molecular basis of epitope-paratope recognition. Our findings explain how *O*-acetyl moieties portray functionality to MenA epitopes and may lead to a profound understanding about protective immunity against MenA.

Results

Generation and Screening of an MenA OS Library for Structural Epitope Mapping. To describe the binding events of a protective MenA mAb toward antigenic MenA OS, a bactericidal murine mAb produced from a MenA conjugate was selected. The mAb was initially obtained by classic hybridoma technology (MenA 1.1, hSBA titer: 0.04 μg/mL; rSBA titer: 0.005 μg/mL; *SI Appendix*, Table S1). For crystallography studies, after mRNA sequencing, codon-optimized cDNA was recombinantly expressed in human Hek293 cells (mAb A1.3, hSBA titer: 0.03 μg/mL; rSBA titer: 0.004 μg/mL; *SI Appendix*, Table S1). Subsequently, a panel of MenA OS fragments was generated by mild hydrolysis of the native PS (Fig. 1*A*). The reaction was quenched when an average degree of polymerization (DP) of 5 was obtained, as confirmed by ^{31}P-NMR (Fig. 1*B*). Single DP fragments were sized by anionic-exchange chromatography (33), allowing the isolation of OSs ranging from DP1 to DP7 (Fig. 1*C*). The identity and acetylation degree (*SI Appendix*, Fig. S1*A* and Table S2) of the produced semisynthetic fragments were confirmed by ^{1}H-NMR spectroscopy (34), which revealed an acetylation degree of 70 to 75% at C-3 and 9 to 12% at C-4. The DP was further corroborated by ^{31}P-NMR and high-performance liquid chromatography with pulsed amperometric detection profiling (35) (*SI Appendix*, Fig. S1*B*).

Length and *O*-Acetylation Dependency of MenA Epitope. The binding of anti-serogroup A murine sera toward the generated oligomers was first assessed by inhibition ELISA, using native PS- coated plates. Preincubation of the polyclonal serum with the OSs of different lengths showed a length-dependent inhibition, with serial dilution of the inhibiting fragments yielding a dose–response curve (*SI Appendix*, Fig. S2 *A* and *B* and Table S3). Of note, DP2 revealed a half maximum inhibitory concentration (IC_{50}) of 8.96×10^{-2} mM, while the introduction of an additional RU (DP3) led to a half-log reduction in the IC_{50} (2.01×10^{-2} mM). A subsequent equivalent but progressive decrease in the IC_{50} was observed from DP3 to DP6 ($IC_{50} = 3.59 \times 10^{-3}$ mM), whereby this fragment inhibited with IC_{50} comparable to fragments longer than 20 RUs (Fig. 2*A*). The selected bactericidal murine mAb showed a similar profile of inhibition as the polyclonal serum (Fig. 2*A* and *SI Appendix*, Fig. S2 *A* and *B*). Remarkably, an increase of 1.5 log was observed between DP6 ($IC_{50} = 4.17 \times 10^{-3}$ mM) and its de-*O*-acetylated congener ($IC_{50} = 1.91 \times 10^{-1}$ mM), revealing that the recognition is largely abolished when the *O*-acetyl moieties are removed.

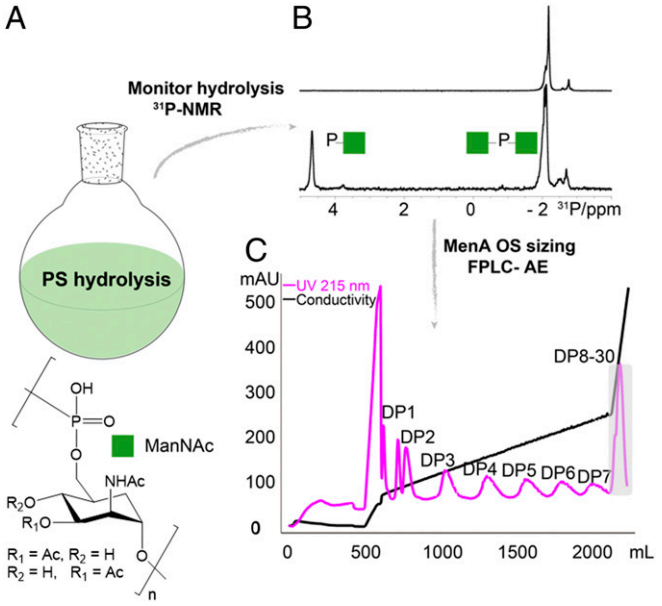

Fig. 1. Hydrolysis and sizing of MenA native PS into a well-defined length OS library. (*A*) Native MenA PS underwent controlled mild acidic hydrolysis. (*B*) Depolymerization was monitored by ^{31}P-NMR. The DP was calculated as $[(P_{Intraglycosidic}/P_{Terminal}) + 1]$. The spectrum of the native MenA PS (*Top*) revealed only the phosphodiester moieties, while the phosphomonoester regions were initially absent due to their lower abundancies. The spectrum of the crude reaction mixture (*Bottom*) exhibited the appearance of the phosphomonoester resonances, confirming the depolymerization of the PS down to an avDP 5. (*C*) Preparative FPLC AEC (Q Sepharose) was used as a size-fractioning step, with a linear gradient of NaCl, to isolate single DP OSs. OSs with longer DPs (gray box) were pooled to originate a population with avDP 20.

Next, the binding kinetics and affinity of different MenA oligomers to the bactericidal mAb A1.3 were characterized by SPR. Biotin neoglycoconjugates were prepared for immobilization on the surface of a streptavidin-coated chip by reductive amination of the OS, followed by acylation with a biotin-active ester (*SI Appendix*, Scheme S1). Of note, the definition of the DP-biotin conjugates considers only the number of unmodified RUs, since the reductive amination procedure used for preparing the neoglycoconjugates leads to the ring opening of the reducing moiety (Fig. 2*B*). The neoglycoconjugates were immobilized at a level ranging from 5 to 10 RU to avoid potential rebinding, and thereafter the mAb was flown over the immobilized OS.

The protective antibody bound to and dissociated from the glycoconjugates with fast on and off rates within nanomolar affinity, revealing a rapid attachment, which could play a role,

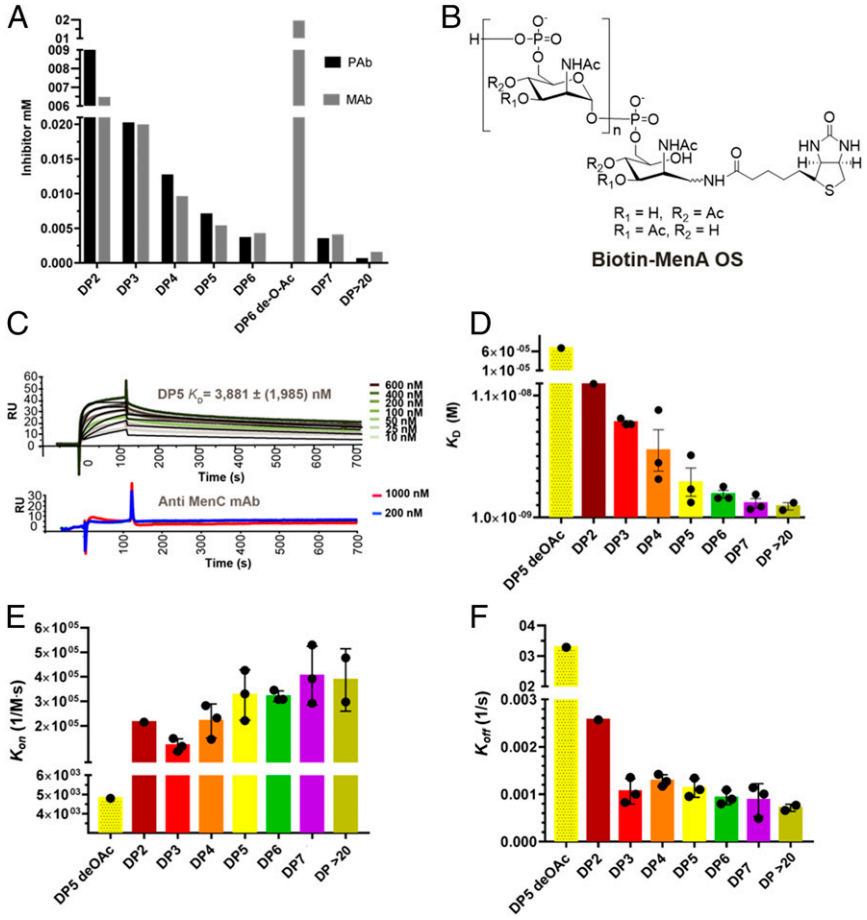

Fig. 2. Competitive ELISA and binding kinetics of a protective mAb to MenA-biotin conjugate OSs of different lengths by SPR. (*A*) Competitve ELISA (IC_{50}) of specific polyclonal serum (black) and monoclonal (gray) antibodies against native MenA PS, as a coating agent, evaluated with MenA OSs of different lengths. Inhibition curves and IC_{50} of the different OSs for polyclonal serum and mAbs are reported in (*SI Appendix*, Fig. S2 *A* and *B* and Table S3). (*B*) Chemical structure of OS-biotin fragments immobilized in streptavidin chips. (*C*) SPR showing a concentration-dependent binding of a protective mAb to MenA DP5-biotin, with no binding observed using a anti-MenC antibody. Binding kinetics and rate constants for OSs of different lengths were inferred by fitting the experimental data with a 1:1 Langmuir binding model. (*D*) Structure of the biotylinated MenA OS and the effect of length on affinity for a range of OSs. (*E* and *F*) On-rate kinetics (M^{-1} s^{-1}) (*E*) shows a gradual increase, while off-rate kinetics (s^{-1}) (*F*) reveals a steep decrease in mAb dissociation when a third RU unit is introduced. Bars represent mean of the data, and the error bars represent the SD of the mean. Values are reported in *SI Appendix*, Table S4, and raw sensorgrams are provided in *SI Appendix*, Figs. S3–S5. A comparison with binding of the Fab is shown in *SI Appendix*, Fig. S6.

especially in environments crowded with PS, such as pathogen cell surfaces, favoring a swift complement-mediated killing of the bacteria. The binding was specific, as demonstrated by the lack of binding with a meningococcal serogroup C mAb (Fig. 2*C*). Dissociation constants were determined using a 1:1 Langmuir binding mode (Fig. 2*C*). The largest increase in affinity was observed from DP2 to DP5 (Fig. 2*D* and *SI Appendix*, Table S4). For the mAb-MenA DP5 complex, we determined a dissociation constant, K_D, of 3.9×10^{-9} ($\pm$ 2.0) M, with a dissociation rate constant, k_{off}, of 1.1×10^{-3} s^{-1} ($\pm$ 0.2) and an association constant, k_{on}, of 3.3×10^{5} ($\pm$ 1.0) $M{\cdot}s^{-1}$. The k_{on} values were very similar for DP2 and DP3 and exhibited a monotonical increase from DP3 to DP6 (Fig. 2*E*), which could be explained by a faster association as a result of greater preorganization of epitopes with increased lengths, since the binding events usually occur with loss of intrinsic conformational flexibility, and, consequently, entropic penalties are likely to have higher contributions for shorter and disordered epitopes (36). On the other hand, k_{off} plateaus at a length of 3 RUs (Fig. 2*E*), suggesting that a trimer accounts for the majority of enthalpic contributions, while additional RUs in longer oligomers are positioned outside of the binding pocket. Overall, the resulting reduction in the K_D value for longer structures could be attributed to a concomitant reduction of conformational entropy penalties, arising from epitope regions conformationally constrained outside the binding pocket (37), while their enthalpy term would remain constant on a length of 3 RUs, since this would suffice to fill the binding pocket. Remarkably, the de-*O*-acetylation of DP5 ($K_D = 6.9 \times 10^{-5}$ M; $k_{off} = 0.3$ s^{-1}; $k_{on} = 4.8 \times 10^{3}$ $M{\cdot}s^{-1}$), resulted in a 4-log increase in dissociation compared with the native DP5. This large abrogation in binding on removal of *O*-acetyl groups confirms the central role of these moieties in the attachment in the ligand-binding groove.

Remarkably, when the binding affinity was measured using the recombinant Fab, the K_D values were 2- to 5-fold lower, depending on the DP tested, compared with those obtained with the mAb (*SI Appendix*, Table S5 and Fig. S6). This clearly indicates that data from the intact antibody were mostly the result of a 1:1 binding modality.

Identification of Antigenic Determinants of Interaction by Solution NMR. To map relevant positions of the MenA oligomers involved in the binding events, considering that the binding affinity optimized at the length of DP6, this OS and its de-*O*-acetyl

congener were selected for STD-NMR epitope mapping (38). Considering that the nM K_D affinity of the acetylated DP6 was due primarily to a low dissociation rate, its spectrum was recorded at a temperature of 303 K to increase the turnover due to tight binding and to minimize avidity. Consistent with the previous observations, the STD-NMR spectrum of DP6 (Fig. 3 *A* and *B*) revealed that methyl protons of the *O*-acetyl groups represent the moieties receiving the highest transfer of saturation (100%), confirming that these determinants are major anchoring points for mAb interactions.

The methyl protons of *N*-acetyl moieties receive a relative 70% saturation, indicating their direct engagement with the antibody as well. Of note, the DP6 is *O*-acetylated at 74% at C-3 and 13% at C-4; thus, 3-*O*-, 4-*O*-, and 2-*N*-acetyls appear strongly engaged in interactions on complex formation. Because of the nanomolar affinity of the DP6, some proton signals of the ring were poorly amplified. To better understand the role of acetylation, the STD-NMR of the de-*O*-Ac DP6 fragment was measured. STD-NMR (Fig. 3*A*) revealed that the proton H4 was receiving a greater amount of saturation (100%), higher than that of H3 (63%), indicating that on removal of the *O*-acetyl groups, position 4 as well as position 3 could be exposed in proximity of the binding pocket. Overall, consistent with the ELISA and SPR data, these results indicate that the acetylation pattern of MenA PS plays a pivotal role in the binding events (Fig. 3*C*).

Structural Insights into the Molecular Mechanism of Recognition of a Protective Epitope. To gain further insight into the molecular basis of recognition, the MenA DP6 OS was also crystallized in complex with the Fab fragment derived from the protective recombinant mAb A1.3 Fab. Crystals of the complex Fab:DP6 diffracted at 2.67 Å resolution. The complex was refined to final R_{work}/R_{free} values of 21%/26.7% (*SI Appendix*, Table S6). Despite the use of a DP6 fragment for the crystallization, additional difference density observed in front of the Fab complementarity determining regions (CDRs) was compatible with the modeling of three RUs. The glycan fragment included in the final structure is herein indicated as a trisaccharide with the three individual RUs identified as A′, B′, and C′ units. Weak electron density beyond the A′ RU departing from the binding pocket suggested that further glycan residues could not be accommodated. Moreover, this residue appears to be 6-phosphorylated at the C′ unit, suggesting that the Fab bound to either the upstream end or an internal fragment, and 1-phosphorylated at the A′ ring, a clear indication that additional residues are extending out of it. A close inspection of the electron density reveals that the trisaccharide is characterized by a variable *O*-acetylation pattern, with the two external A′ and C′ units acetylated at C-3 and the central and most buried B′ unit acetylated at C-4 (Fig. 4 *A* and *B*).

Electron density maps of the Fab fragment were of good overall quality, allowing the modeling of residues Q1 to C129 and G134 to G215 from the H-chain and residues D1 to N217 from the L-chain of the molecules' HL and MN copies. In the case of the OP molecule, no clear electron density was visible on the constant regions (i.e., residues V112 to G215 of the H-chain and E110 to N217 of the L-chain).

Pairwise structural superimposition among the different copies of the complex present in the asymmetric unit resulted in an overall Cα rmsd value of 0.276 Å (Cα rmsd of 0.305 Å in the CDRs); therefore, they were considered essentially identical within the limits of experimental error. The mean pairwise rmsd in the atomic positions of the three trisaccharide copies bound to the Fab was 0.33 Å, indicating that the conformation of the

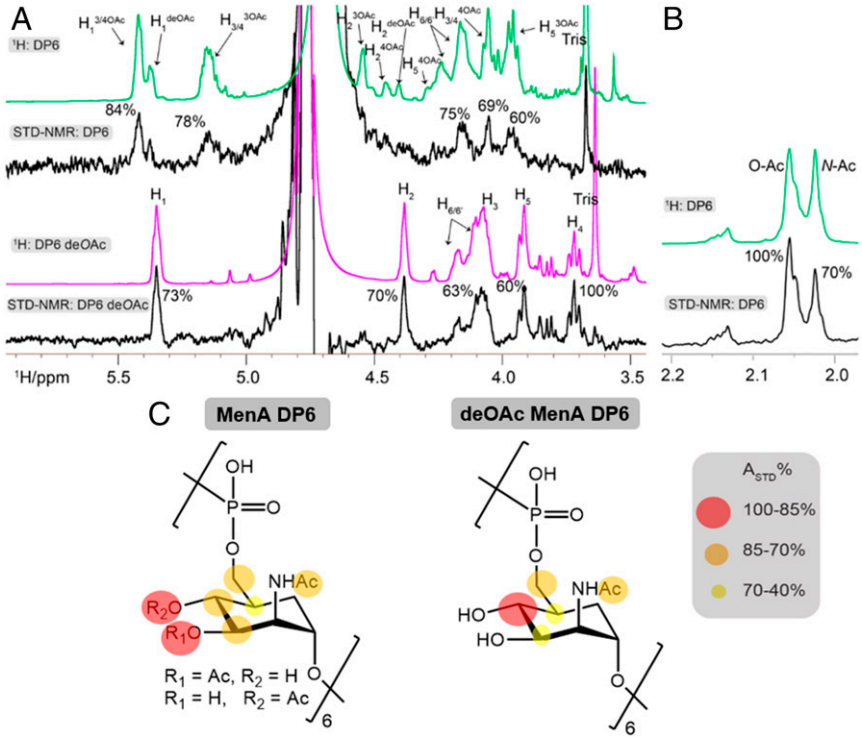

Fig. 3. Epitope mapping of MenA DP6 and de-*O*-Ac-DP6 OS complexed with a mAb by STD NMR. (*A*) Native MenA DP6 (green) and de-*O*-Ac-DP6 (magenta) STD-NMR spectra were run with a 1:100 mAb/OS mixture. The irradiation frequency was set at 7.00 ppm, and a saturation time of 2 s was used (t = 303 K for DP6 and 298 K for de-*O*-Ac-DP6). All STD intensities were normalized against the *O*-acetyl moiety. (*B*) Zoomed-in view of the acetyl region of DP6 (green). (*C*) Color code indicating the magnitude of the normalized intensities: red, 100 to 85%; orange, 85 to 70%; yellow, 70 to 40%).

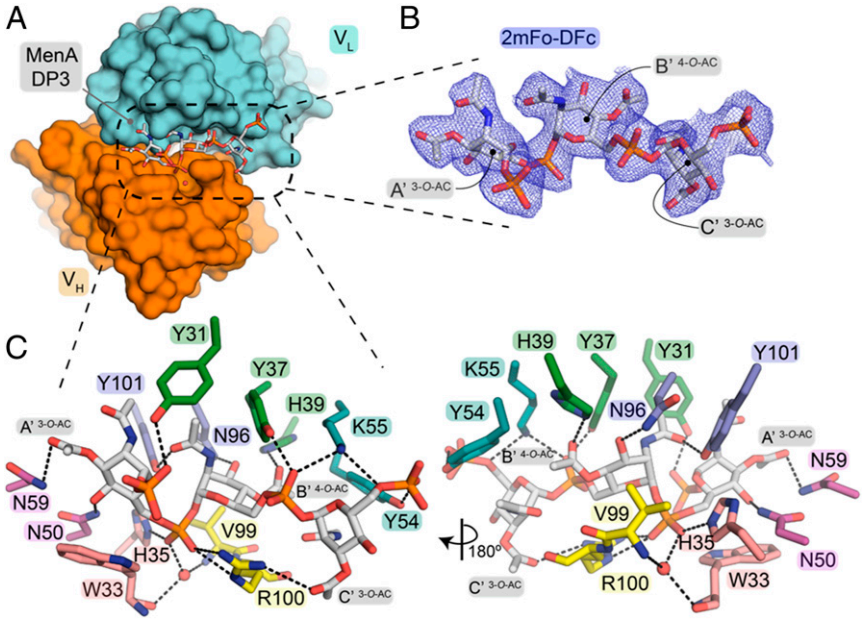

Fig. 4. X-ray crystallographic structure of the Fab in complex with a MenA trisaccharide. (*A*) Surface representation of the variable light (VL) and heavy chain (VH) of the Fab, colored in cyan and orange, respectively. MenA trisaccharide, represented as gray sticks, is located at the interface between the heavy chain and light chain CDRs. (*B*) 2m*Fo*-D*Fc* electron density map (blue mesh, contoured at 1.0 σ) of the modeled MenA trisaccharide fragment bound to the Fab. The trimer exhibits a 3-*O*-acetylation in units A′ and C′ and 4-*O*-acetylation in unit B′. (*C*) Zoomed-in view (*Left*) and 180° rotation (*Right*) of the interactions of MenA trisaccharide with the different CDR residues depicted in sticks, with a color-coding scheme reflecting the CDR classification (CDR L1, green; CDR L2, teal; CDR L3, blue; CDR H1, pink; CDR H2, magenta; CDR L3, yellow) according to North et al. (39) (*SI Appendix*, Fig. S8).

saccharide is also highly similar. Consequently, one copy (MN) was used for the description of the structure.

The antigen-binding site is a small linear groove in the interface of CDR L1-L3 and CDR H1-H3 (Fig. 4*A*) with approximate dimensions of 21.4 Å long, 8.6 Å wide, and 8.4 Å deep. All three RUs of the trisaccharide are involved in multiple interactions with the antibody (Fig. 4 *C* and *D*). The RU B′ is mostly engulfed between CDR L1 and L3 and CDR H1 and H3, accounting for the majority of intermolecular contacts on complex formation. Within a secondary shallower binding pocket formed by CDR L1 and L3 and CDR H1 and H2 is the RU A′, whereas the RU C′′ makes most of its contacts with CDR L2 and H3 and is the region of the ligand mostly exposed to the solvent, consistent with its higher levels of B factors (*SI Appendix*, Fig. S7). The light-chain leaflet CDR is dominated by aromatic side chains (Y31, Y37, H39, Y54, F60, and Y101) (Fig. 4*C*, *Right*), while the heavy-chain CDR is populated by polar side chains—i.e., two Asn residues (N50, N59) and some positively charged residues (R100 and H35) (Fig. 4*C*, *Left*)—in a complementary interplay with the electropositive patches of the glycan, notably in the methyl groups of the *O*-acetyl and *N*-acetyl substituents, and its overall hydrophilic character (*SI Appendix*, Fig. S8). Crucially, the positive electrostatic potential along the CDR moieties in the hypervariable domains of the Fab contributes to the electrostatic attraction of the MenA trisaccharide backbone phosphodiester, most likely resulting in an increased capacity of the Fab to attract the negatively charged phosphodiester moieties.

The glycan RU B′ establishes the largest number of interactions, donating a H-bond to the side chain N96 (L) through its 3-OH group, while the carbonyl of the 4-*O*-acetyl moiety accepts a H-bond from H39 (L). In addition, the 2-*N*-acetyl carbonyl moiety accepts a H-bond from the phenol side chain of Y101 (L). Importantly, the electron-withdrawing character of the B′ 2-*N*-acetyl group leads to a polarization effect on the methyl groups, which become more acidic. These polarized methyl groups are within 4 Å of residues Y31 (L) and Y37 (L) and act as good CH-π donors (40, 41). Conversely, these aromatic side chains are in turn involved in an extended network of H-bonds. Remarkably, Y31 (L) donates a H-bond to the A′ 1-phosphate group, whereas Y37 (L) donates a H-bond to the phosphodiester appended between the subunits B′ and C′, which is engaged in a bidentate H-bond with electropositive K55 (L), resulting in increased

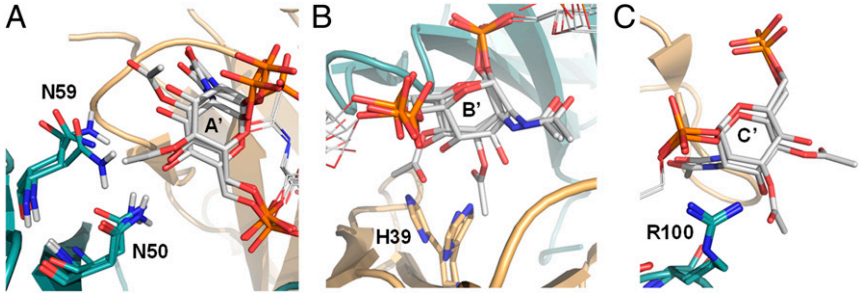

Fig. 5. Docked-minimized structures of complexes between bactericidal mAb and MenA DP3 OS with different *O*-acetylation patterns. The amino acids differing in their interaction with 4-OAc, 3-Oac, and de-OAc units of the three residues A′ (*A*), B′ (*B*), and C′ (*C*) of MenA trisaccharide are indicated.

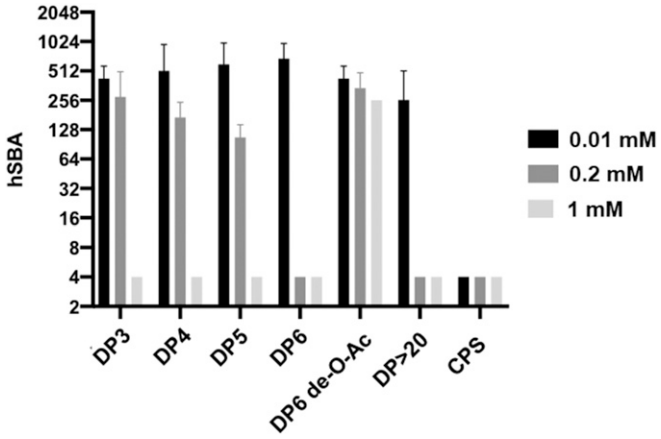

Fig. 6. Inhibition of human SBA using MenA fragments of different lengths. Inhibitors at different concentrations were preincubated with pooled human immune serum, followed by exposure to a bacterial strain in the presence of human complement. Bars represent mean values, and the error bars represent the SD of the mean from triplicate experiments.

electronegativity of the former π-system, making them good CH-π acceptors (42).

Concerning the glycan RU A′, the 3-*O*-acetyl ether group receives a H-bond from the N59 (H) amide side chain, whereas the OH-4 acts as a H-bond acceptor from the N50 (H) amide side chain. Of note, the closely positioned H35 (H) donates a H-bond to the phosphodiester appended between the subunits A′ and B′, which in turn makes a second H-bond with a coordinated water molecule bridging two additional H-bonds to the W33 (H) and V99 (H) backbone carbonyl and amine groups, respectively. Although no major interactions are established by the A′ 2-*N*-acetyl group and the binding pocket, the former amide is positioned well to establish an intramolecular H-bond with the B′ 2-*N*-acetyl group carbonyl group.

Finally, concerning the glycan RU C′, the 3-*O*-acetyl carbonyl moiety is within H-bond distance from the guanidino group of R100 (H) residue. As previously described for unit B′, the polarized methyl group of 2-*N*-acetyl moiety is involved in a CH–π interaction with the Y54 (L) residue, with the latter further engaged in a H-bond with the terminal C′ 6-phosphate group.

In Silico Docking Experiments of Different *O*-Acetylation Patterns. Interestingly, the *O*-acetyl groups are involved in several interactions within the binding pocket, and their presence affects the H-bond network established with the Fab fragment. Although the crystallized complex shows a 3-4-3 *O*-acetylation pattern in the trisaccharide epitope, the natural PSs present multiple combinatorial possibilities of *O*-acetylation. Thus, we asked whether alternative patterns of *O*-acetylation would still result in stable interactions with the bactericidal mAb.

Docking-minimization protocols performed for the complexes formed between the Fab and diverse 3-mer with different acetylation patterns identified de-*O*-acetyl, 3-*O*-acetyl, and 4-*O*-acetyl OSs as potential ligands (Fig. 5*A* and *SI Appendix*, Figs. S9 and S10). According to the calculations, the complexes were conformationally stable, and most of the stabilizing contacts were maintained. However, acetylation in certain positions allowed the establishment of additional interactions with the antibody, which in turn could provide an increased binding affinity. In particular, the contacts between unit B′ and H39 (L) are maintained after minimization irrespective of the acetylation pattern (Fig. 5*B*). Modeled complexes with either Nε2-H or Nδ1-H tautomeric states for H39 (L) showed key contacts between OH in positions 3 and 4 and the imidazole ring of that residue, which was easily relocated depending on the acetylation pattern. In contrast, the 3-*O*-acetyl group of C′ was key to maintaining the contacts with R100 (H), and their absence or shift to position 4 would abolish this interaction (Fig. 5*C*). Similarly, deacetylation of unit A′ would statistically diminish the number of hydrogen bond acceptor atoms able to interact with N59 (H) and N50 (H) (Fig. 5*C* and *SI Appendix*, Fig. S9).

Preferential Recognition of *O*-Acetylated Glycotope by Human Polyclonal Serum. To explore whether the mapped acetylated trisaccharide epitope is representative of the immune response elicited in humans by MenA conjugate, a competitive serum bactericidal activity (SBA) assay was conducted (43). To this end, human sera, elicited by immunization with the MenACWY-CRM_{197}

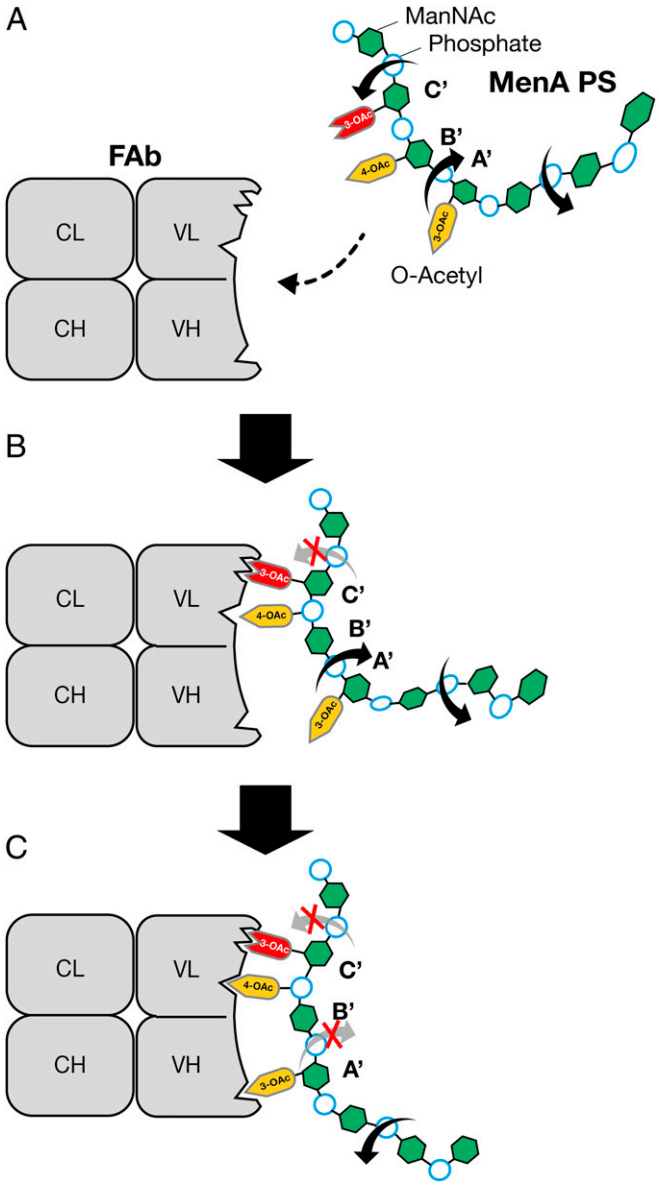

Fig. 7. Model of interaction of the trimer epitope mapped out of the hexamer structure and impact of *O*-acetylation pattern. 3-*O*-acetylation at C′ residue (red labeled) seems crucial for binding (*A*), and thus could trigger a more rigid initial interaction of this residue. Variable *O*-acetylation patterns (yellow) appear acceptable in the A′ and B′ RUs, suggesting that those residues could rotate (*B*) until they find proper engagement with the binding pocket (*C*).

vaccine, was preincubated with diverse inhibitors at different concentrations, followed by evaluation of their human complement-mediated bactericidal activity.

Fragments with a length of DP3 to DP5 were able to inhibit complement- mediated killing of meningococcus at a concentration of 1 mM (Fig. 6). In contrast, DP6 substantially inhibited the sera from binding to the pathogen capsule at a lower concentration of 0.2 mM, similar to DP20 and PS. Conversely, de-*O*-acetyl DP6 did not provide SBA inhibition (Fig. 6). These data indicate that DP3 is the minimal length antigenic epitope recognized by immune human sera, and that lengths longer than DP5 show higher serum depletion because of increased avidity.

Discussion

Glycoconjugate vaccines are a well-established means of eliciting protective antibodies toward PS surrounding the surface of pathogens (44). Despite this success, however, elucidation of the molecular basis of recognition of antigenic glycan epitopes by bactericidal antibodies at atomic resolution remains a challenge in structural glycobiology (45). Owing to the refractory nature of glycans to crystallize, information on the structural requirements of antigen recognition has been mainly gathered via combinations of various techniques, including SPR, isothermal titration calorimetry, NMR spectroscopy (46–52), and, more recently, single particle cryo-electron microscopy (53, 54).

Here we showcase an integrated approach to map, at atomic detail, the minimal antigenic epitope of the MenA capsular PS, uncovering with unprecedented detail the length and *O*-acetyl pattern engaged in molecular recognition with a bactericidal mAb. *O*-acetylation has been hypothesized to be an important attribute for meningococcal vaccine efficacy (30). Inhibition ELISA with anti-MenA polyclonal serum and a bactericidal mAb showed a length-dependent recognition. Importantly, a trimer portion of the PS was sufficient to establish strong binding. In agreement with these data, SPR showed dissociation kinetics decreasing progressively from DP2 to DP5, with the off-rate kinetics reaching a plateau for fragments longer than 3 RUs. On the other hand, de-*O*-acetylated DP5 resulted in abrogation of its binding. STD-NMR experiments unraveled a preferential transfer of saturation toward both *O*- and *N*-acetyl groups, thereby confirming their engagement on complex formation.

Consistent with these findings, the crystal structure of the Fab:DP6 complex solved at 2.67 Å resolution revealed a trimer antigenic determinant adopting a linear bound conformation, with an alternating 3-4-3 *O*-acetylation pattern. The antigen recognition is governed by several types of interactions with different natures, mainly H-bonds, hydrophobic and electrostatic interactions, and van der Waals forces. Fittingly, the binding pose reveals that all *O*-acetyl moieties are engaged in H-bond networks, and docking studies with deacetylated MenA homologs highlight their relevance in the interaction, while all but one *N*-acetyl are interacting with the bactericidal mAb.

Remarkably, while the 3-*O*-acetyl of the C′ glycan residue seems to confer a greater specificity in engagement of the binding pocket, A′ and B′ moieties show greater promiscuity toward other *O*-acetylation patterns, thus conferring a higher plasticity to the mAb (Fig. 7). Furthermore, the resolved trimer was part of a longer structure, of which the mAb bound to either an internal position or an upstream portion. The Ab recognition does not seem to affect the canonical conformation of the sugar in solution.

Finally, the human complement-mediated bactericidal activity of sera from previously vaccinated subjects was efficiently inhibited by fragments with lengths of 3 to 5 RUs, although higher inhibitory concentrations were needed compared with DP6 and fragments longer than DP20 because of their lower avidity. In contrast, a de-*O*-acetylated DP6 was not able to inhibit the serum bactericidal activity, confirming that vaccine-induced immune responses in humans are also directed to the *O*-acetylated trimer epitope.

Our findings clearly demonstrate that the *O*-acetylated trimer MenA epitope is involved in the molecular recognition of antibodies elicited by immunization with MenA PS-based vaccines and likely by preexposition to the heavily encapsulated meningococcus. While the epitope is a short trimer, our data also show that its multimeric exposition in the polysaccharide capsule favors avidity interactions that further strengthen antibody binding and aid complement deposition. The unique features of the antigenic determinant of MenA capsular PS elucidated by this study add to our understanding of the molecular basis of the immune recognition of carbohydrate haptens and pave the way for the rational design of improved vaccines (17) and therapeutics (9).

Materials and Methods

Recombinant murine Fab was purified in 20 mM PBS and 150 mM NaCl pH 7.1 and then concentrated to 15 mg/mL using a centrifugal device with a 10-kDa cutoff membrane (Amicon Ultra; Millipore Sigma). The complex between DP6 and the Fab was prepared by incubation at 4 °C (10:1 molar ratio of saccharide:Fab) and then subjected to crystallization trials using a Crystal Gryphon liquid handling robot (Art Robbins Instruments). Details of the crystallization of the complex are reported in *SI Appendix*.

Competitive SBA was performed with pooled human antibodies obtained via a Phase II clinical trial V102_02 (ClinicalTrials.gov identifier NCT01210885) conducted at multiple sites (Panama and Chile) with Menveo vaccine under the approval of the local Ethical Committee. The samples, which were obtained on written informed consent from study participants, were deidentified before use in the reported analysis. The experimental protocol is described in *SI Appendix*.

Experimental methods for OS generation, inhibition ELISA, SPR measurements, STD NMR experiments, cocrystallization of the Fab-glycan complex, and in silico modeling are provided in *SI Appendix*.

Data Availability. All study data are included in the main text and *SI Appendix*.

ACKNOWLEDGMENTS. We thank Barbara Brogioni and Cristiana Balocchi (GSK) for their work, which included, respectively, assessing the polymerization level of the MenA fragments and testing the bactericidal activity of mAbs, leading to the selection of the recombinant one further characterized in this work. Without their contributions, the work described here would not have been possible. We also thank Elena Mori and Daniele Veggi (GSK) for the helpful discussions on meningococcal antibody responses and X-ray crystallography, respectively. Giorgio Corsi is acknowledged for the artwork. We thank the European Synchrotron Radiation Facility for providing the synchrotron radiation facilities and the staff at beamline ID30B for technical assistance with data collection. This work was sponsored by GlaxoSmithKline Biologicals and has received funding from the European Union's Horizon 2020 Research and Innovation Programme under the Marie Skłodowska-Curie Grant Agreement 675671.

1. G. Ada, D. Isaacs, Carbohydrate-protein conjugate vaccines. *Clin. Microbiol. Infect.* **9**, 79–85 (2003).
2. P. Costantino, R. Rappuoli, F. Berti, The design of semi-synthetic and synthetic glycoconjugate vaccines. *Expert Opin. Drug Discov.* **6**, 1045–1066 (2011).
3. C. Anish, B. Schumann, C. L. Pereira, P. H. Seeberger, Chemical biology approaches to designing defined carbohydrate vaccines. *Chem. Biol.* **21**, 38–50 (2014).
4. F. Broecker *et al*., Multivalent display of minimal Clostridium difficile glycan epitopes mimics antigenic properties of larger glycans. *Nat. Commun.* **7**, 11224 (2016).
5. B. Schumann *et al*., Development of an efficacious, semisynthetic glycoconjugate vaccine candidate against Streptococcus pneumoniae Serotype 1. *ACS Cent. Sci.* **4**, 357–361 (2018).
6. A. Gimeno, P. Valverde, A. Ardá, J. Jiménez-Barbero, Glycan structures and their interactions with proteins. A NMR view. *Curr. Opin. Struct. Biol.* **62**, 22–30 (2020).
7. R. Marchetti *et al*., Burkholderia pseudomallei capsular polysaccharide recognition by a monoclonal antibody reveals key details toward a biodefense vaccine and diagnostics against melioidosis. *ACS Chem. Biol.* **10**, 2295–2302 (2015).
8. M. Tamigney Kenfack *et al*., Deciphering minimal antigenic epitopes associated with Burkholderia pseudomallei and Burkholderia mallei lipopolysaccharide O-antigens. *Nat. Commun.* **8**, 115 (2017).
9. C. Soliman, G. B. Pier, P. A. Ramsland, Antibody recognition of bacterial surfaces and extracellular polysaccharides. *Curr. Opin. Struct. Biol.* **62**, 48–55 (2020).

10. M. Cygler, D. R. Rose, D. R. Bundle, Recognition of a cell-surface oligosaccharide of pathogenic Salmonella by an antibody Fab fragment. *Science* **253**, 442–445 (1991).
11. S. Villeneuve *et al*., Crystal structure of an anti-carbohydrate antibody directed against Vibrio cholerae O1 in complex with antigen: Molecular basis for serotype specificity. *Proc. Natl. Acad. Sci. U.S.A.* **97**, 8433–8438 (2000).
12. B. Vulliez-Le Normand *et al*., Structures of synthetic O-antigen fragments from serotype 2a Shigella flexneri in complex with a protective monoclonal antibody. *Proc. Natl. Acad. Sci. U.S.A.* **105**, 9976–9981 (2008).
13. T. Murase *et al*., Structural insights into antibody recognition of mycobacterial polysaccharides. *J. Mol. Biol.* **392**, 381–392 (2009).
14. F. Carboni *et al*., Structure of a protective epitope of group B Streptococcus type III capsular polysaccharide. *Proc. Natl. Acad. Sci. U.S.A.* **114**, 5017–5022 (2017).
15. J. Guiard, E. Paszkiewicz, J. Sadowska, D. R. Bundle, Design and synthesis of a universal antigen to detect brucellosis. *Angew. Chem. Int. Ed.* **52**, 7181–7185 (2013).
16. P. H. Seeberger, D. B. Werz, Synthesis and medical applications of oligosaccharides. *Nature* **446**, 1046–1051 (2007).
17. Q. Gao *et al*., Immunoactivity of protein conjugates of carba analogues from Neisseria meningitidis a capsular polysaccharide. *ACS Chem. Biol.* **8**, 2561–2567 (2013).
18. S. Fallarini *et al*., A synthetic disaccharide analogue from Neisseria meningitidis A capsular polysaccharide stimulates immune cell responses and induces immunoglobulin G (IgG) production in mice when protein-conjugated. *ACS Infect. Dis.* **1**, 487–496 (2015).
19. L. Lapeyssonnie, Cerebrospinal meningitis in Africa. *Bull. World Health Organ.* **28**, 1–114 (1963).
20. L. H. Harrison, C. L. Trotter, M. E. Ramsay, Global epidemiology of meningococcal disease. *Vaccine* **27**, B51–B63 (2009).
21. F. Marc LaForce, N. Ravenscroft, M. Djingarey, S. Viviani, Epidemic meningitis due to group A Neisseria meningitidis in the African meningitis belt: A persistent problem with an imminent solution. *Vaccine* **27**, B13–B19 (2009).
22. K. Tiffay, L. Jodar, M.-P. Kieny, M. Socquet, F. M. LaForce, The evolution of the meningitis vaccine project. *Clin. Infect. Dis.* **61** (suppl. 5), S396–S403 (2015).
23. C. L. Trotter *et al*., Impact of MenAfriVac in nine countries of the African meningitis belt, 2010-15: An analysis of surveillance data. *Lancet Infect. Dis.* **17**, 867–872 (2017).
24. T. Y. Liu, E. C. Gotschlich, E. K. Jonssen, J. R. Wysocki, Studies on the meningococcal polysaccharides, I: Composition and chemical properties of the group A polysaccharide. *J. Biol. Chem.* **246**, 2849–2858 (1971).
25. D. R. Bundle, I. C. Smith, H. J. Jennings, Determination of the structure and conformation of bacterial polysaccharides by carbon 13 nuclear magnetic resonance. Studies on the group-specific antigens of Neisseria meningitidis serogroups A and X. *J. Biol. Chem.* **249**, 2275–2281 (1974).
26. X. Lemercinier, C. Jones, Full 1H NMR assignment and detailed O-acetylation patterns of capsular polysaccharides from Neisseria meningitidis used in vaccine production. *Carbohydr. Res.* **296**, 83–96 (1996).
27. P. Costantino *et al*., Development and phase 1 clinical testing of a conjugate vaccine against meningococcus A and C. *Vaccine* **10**, 691–698 (1992).
28. L. A. Mulard, "Bacterial polysaccharides as major surface antigens: Interest in O-acetyl substitutions" in *Carbohydrate Chemistry: Chemical and Biological Approaches 43*, A. P. Rauter, T. Lindhorst, Queneau Y, Eds. (The Royal Society of Chemistry, 2018), pp. 71–103.
29. F. Berti, R. De Ricco, R. Rappuoli, Role of O-acetylation in the immunogenicity of bacterial polysaccharide vaccines. *Molecules* **23**, 1340 (2018).
30. D. S. Berry, F. Lynn, C.-H. Lee, C. E. Frasch, M. C. Bash, Effect of O acetylation of Neisseria meningitidis serogroup A capsular polysaccharide on development of functional immune responses. *Infect. Immun.* **70**, 3707–3713 (2002).
31. J. Hlozek, M. M. Kuttel, N. Ravenscroft, Conformations of Neisseria meningitidis serogroup A and X polysaccharides: The effects of chain length and O-acetylation. *Carbohydr. Res.* **465**, 44–51 (2018).
32. I. Calloni *et al*., The conformation of the mannopyranosyl phosphate repeating unit of the capsular polysaccharide of Neisseria meningitidis serogroup A and its Carba-Mimetic. *Eur. J. Org. Chem.* **2018**, 4548–4555 (2018).
33. P. Costantino *et al*., Size fractionation of bacterial capsular polysaccharides for their use in conjugate vaccines. *Vaccine* **17**, 1251–1263 (1999).
34. C. Jones, X. Lemercinier, Use and validation of NMR assays for the identity and O-acetyl content of capsular polysaccharides from Neisseria meningitidis used in vaccine manufacture. *J. Pharm. Biomed. Anal.* **30**, 1233–1247 (2002).
35. F. Berti *et al*., Relative stability of meningococcal serogroup A and X polysaccharides. *Vaccine* **30**, 6409–6415 (2012).
36. G. Klebe, Applying thermodynamic profiling in lead finding and optimization. *Nat. Rev. Drug Discov.* **14**, 95–110 (2015).
37. A. Gimeno *et al*., Minimizing the entropy penalty for ligand binding: Lessons from the molecular recognition of the histo blood-group antigens by human Galectin-3. *Angew. Chem. Int. Ed.* **58**, 7268–7272 (2019).
38. M. Mayer, B. Meyer, Characterization of ligand binding by saturation transfer difference NMR spectroscopy. *Angew. Chem. Int. Ed.* **38**, 1784–1788 (1999).
39. B. North, A. Lehmann, R. L. J. Dunbrack Jr, A new clustering of antibody CDR loop conformations. *J. Mol. Biol.* **406**, 228–256 (2011).
40. J. L. Asensio, A. Ardá, F. J. Cañada, J. Jiménez-Barbero, Carbohydrate-aromatic interactions. *Acc. Chem. Res.* **46**, 946–954 (2013).
41. L. Unione *et al*., Fluoroacetamide moieties as NMR spectroscopy probes for the molecular recognition of GlcNAc-containing sugars: Modulation of the CH-π stacking interactions by different fluorination patterns. *Chemistry* **23**, 3957–3965 (2017).
42. K. L. Hudson *et al*., Carbohydrate–aromatic interactions in proteins. *J. Am. Chem. Soc.* **137**, 15152–15160 (2015).
43. R. Borrow, P. Balmer, E. Miller, Meningococcal surrogates of protection—Serum bactericidal antibody activity. *Vaccine* **23**, 2222–2227 (2005).
44. E. De Gregorio, R. Rappuoli, From empiricism to rational design: A personal perspective of the evolution of vaccine development. *Nat. Rev. Immunol.* **14**, 505–514 (2014).
45. O. Haji-Ghassemi, R. J. Blackler, N. Martin Young, S. V. Evans, Antibody recognition of carbohydrate epitopes. *Glycobiology* **25**, 920–952 (2015).
46. T. Peters, B. M. Pinto, Structure and dynamics of oligosaccharides: NMR and modeling studies. *Curr. Opin. Struct. Biol.* **6**, 710–720 (1996).
47. A. Ardá, J. Jiménez-Barbero, The recognition of glycans by protein receptors. Insights from NMR spectroscopy. *Chem. Commun. (Camb.)* **54**, 4761–4769 (2018).
48. P. Valverde, J. I. Quintana, J. I. Santos, A. Ardá, J. Jiménez-Barbero, Novel NMR avenues to explore the conformation and interactions of glycans. *ACS Omega* **4**, 13618–13630 (2019).
49. C. Rademacher *et al*., Ligand specificity of CS-35, a monoclonal antibody that recognizes mycobacterial lipoarabinomannan: A model system for oligofuranoside-protein recognition. *J. Am. Chem. Soc.* **129**, 10489–10502 (2007).
50. Q. Zhang *et al*., Synthetic, zwitterionic Sp1 oligosaccharides adopt a helical structure crucial for antibody interaction. *ACS Cent. Sci.* **5**, 1407–1416 (2019).
51. M. A. Oberli *et al*., Molecular analysis of carbohydrate-antibody interactions: Case study using a Bacillus anthracis tetrasaccharide. *J. Am. Chem. Soc.* **132**, 10239–10241 (2010).
52. J. Boutet *et al*., Detailed investigation of the immunodominant role of O-antigen stoichiometric O-acetylation as revealed by chemical synthesis, immunochemistry, solution conformation and STD-NMR spectroscopy for Shigella flexneri 3a. *Chemistry* **22**, 10892–10911 (2016).
53. D. Oyen *et al*., Cryo-EM structure of P. falciparum circumsporozoite protein with a vaccine-elicited antibody is stabilized by somatically mutated inter-Fab contacts. *Sci. Adv.* **4**, eaau8529 (2018).
54. M. A. Tortorici *et al*., Structural basis for human coronavirus attachment to sialic acid receptors. *Nat. Struct. Mol. Biol.* **26**, 481–489 (2019).